ACS APPLIED MATERIALS & INTERFACES

RESEARCH ARTICLE

www.acsami.org

Fabrication of nanoporous Cu−Pt(Pd) core/shell structure by galvanic replacement and its application in electrocatalysis

Caixia Xu,*[,†] Yunqing Liu,[†] Jinping Wang,[†] Haoran Geng,[†] and Huajun Qiu*[,‡,§]

[†]Key Laboratory of Chemical Sensing & Analysis in Universities of Shandong, Department School of Chemistry and Chemical Engineering, University of Jinan, Jinan 250022, China

[‡]Qingdao Institute of Bioenergy and Bioprocess Technology, Chinese Academy of Sciences, Qingdao 266101, China

[§]School of Chemistry and Chemical Engineering, Shandong University, Jinan 250100, China

ABSTRACT: We describe a general strategy to fabricate a new type of nanoporous core/shell structured bimetallic nanocomposites with controllable metal components. Nanoporous copper (NPC) obtained by dealloying Cu/Al alloy is used as both reducing agent and three-dimensional substrate. Electron microscope and X-ray diffraction characterizations demonstrated that a simply galvanic-replacement reaction with H_2PtCl_6 aqueous solution can easily generate nanoporous core/shell structure with a thin Pt/Cu alloy shell and Cu (or Pt/Cu alloy) core. The morphology and crystal structure evolution of the nanocomposites are studied and discussed in detail. The as-prepared bimetallic PtCu nanocomposites show greatly enhanced catalytic activity and stability toward methanol electro-oxidation as compared with commercial Pt/C catalyst. This facile in situ preparation strategy is also suitable for large-scale production of this novel and inexpensive catalyst.

KEYWORDS: nanoporous, core−shell, methanol, electrocatalyst, fuel cell

INTRODUCTION

Pt group-based catalysts are of central importance in industrial catalysis and green energy technologies, such as fuel cells.[1−10] Many efforts have been made to prepare various kinds of Pt- and Pd-based nanomaterials in order to improve the catalytic activities of these precious metals and their utilization. These nanomaterials are usually Pt (Pd)-based alloys, core/shell structure with non-precious component as core and precious metals as shell, and heteoaggregates.[5−16] Particularly, the core/shell structure has been widely studied. For example, by galvanic displacement of a Cu monolayer (underpotential deposited), Adzic's group has successfully prepared a series of core/shell structure with Pt-shell and different cores.[11−14] However, the preparation of these nanomaterials are relatively complicated and in order to obtain the desired structure, great care is needed. Therefore, it would be interesting and important to develop a convenient and environmentally benign approach to prepare the core/shell nanostructures.

Recently, nanoporous metals with three-dimensional (3D) bicontinuous pore-ligament structure obtained by dealloying have aroused great interest.[17] These nanoporous metals with high surface area do have some advantages over nanoparticles: (1) they are free-standing and free of particle agglomeration; (2) they can be easily prepared, reproduced and employed; (3) prepared in concentrated acidic or alkaline solution (without any surfactants), the surface of the nanoporous metals is extremely clean. Nanoporous metal such as nanoporous gold (NPG, obtained by dealloying AgAu[18−22]) has been demonstrated to be good catalyst for CO, glucose oxidation,[19,20] and methanol electro-oxidation[21] because of their special physicochemical properties. Considering that nanoporous Au or Pt comprises pure precious metal and their catalytic activities are mainly from ligament surface atoms, we think that it is of practical importance to prepare nanoporous metal with a non-precious metal as a 3D skeleton of nanoporosity and a nanometer-thick precious metal decorated on the ligament surfaces of the nanoporous non-precious metal. In this way, the precious metals get better used (commercially) and the core/shell nanostructure may further improve the catalytic performance of the precious metals.

In our previous work, nanoporous copper (NPC, obtained by dealloying CuAl alloy) has been demonstrated to be a good 3D skeleton of nanoporosity.[23−28] By a simple replacement reaction between NPC and noble metal salts (H_2PtCl_6 or K_2PdCl_4), we have successfully prepared novel Pt- or Pd-based nanotubular mesoporous bimetallic materials.[23,24] In the present work, by controlling the rate of the replacement reaction (i.e., by simply changing the concentration of the noble metal salts), it is interesting to find that this approach can be modified to prepare core/shell nanostructure with a thin layer of noble metal-based alloy as shell and non-noble metal (or alloy) as core (the 3D bicontinuous pore-ligament structure is well maintained). Detailed electrochemical studies show that the as-made nanoporous Cu/Pt core/shell structures have much improved catalytic activity and stability toward methanol electro-oxidation as compared with state-of-the-art Pt/C catalyst.

EXPERIMENTAL SECTION

$Cu_{25}Al_{75}$ alloy foils were made by refining high-purity (99.9 %) Cu and Al in an arc-furnace, followed by melt-spinning under N_2-protected atmosphere. NPC was prepared by dealloying $Cu_{25}Al_{75}$ alloy foils in 1 M NaOH for 5 h at room temperature. Nanoporous Pt-based core/shell structured nanocomposites were prepared by adding 8 mg NPC into 120 mL H_2PtCl_6 aqueous solution (0.8 mM) in a three-neck flask at 5 °C under N_2-protected magnetic stirring conditions. The Pd-based core/shell structure was prepared in the same way by adding 8 mg NPC into

Received: August 7, 2011
Accepted: October 28, 2011
Published: October 28, 2011

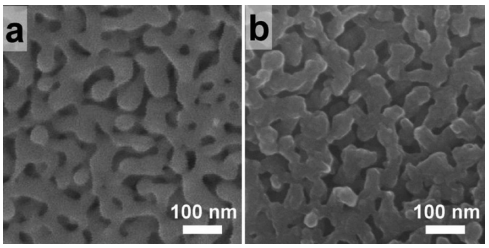

Figure 1. SEM images of as-prepared NPC (a) before and (b) after reacted with 0.8 mM H_2PtCl_6 solution for 60 min.

120 mL of K_2PdCl_4 solution (2.5 mM) in a three-neck flask at 5 °C under N_2-protected magnetic stirring conditions.

X-ray diffraction was collected on a Bruker D8 advanced X-ray diffractometer using Cu KR radiation (λ = 1.5418 Å) at a step rate of 0.02°/s. The microstructures of all samples were characterized on a JEOL JSM-6700F field-emission scanning electron microscope, equipped with an Oxford INCA x-sight energy-dispersive X-ray spectrometer and a JEM-2100 high-resolution transmission electron microscope.

The catalyst suspensions were made by mechanically mixing 4.0 mg nanoporous nanocomposite catalysts powder, 4.0 mg carbon powder, 300 μL isopropanol, and 100 μL Nafion solution (5 wt %). The mixture was sonicated for 30 min to form a uniform suspension. The catalyst suspension (3 μL) was placed on a polished glassy carbon electrode (GCE, 4 mm in diameter) and dried. Prior to each measurement, the electrolytes were deoxygenated with high-purity N_2 for at least 30 min. Considering that certain Cu atoms on the nanocomposite surface may be unstable in the electrochemical environment, all the electrocatalytic measurements were recorded after the modified electrodes reached the steady-state by ~10 potential cycling from 0 to 1.3 V (vs. RHE) in 0.5 M H_2SO_4 solution. CO-stripping experiments were performed by first holding the as-prepared electrode at 0.15 V (vs. RHE) in a 0.5 M H_2SO_4 solution with continuous CO bubbling for ca. 20 min. Then, the electrode was transferred into a N_2-purged 0.5 M H_2SO_4 solution to record the CO-stripping profile.

All electrochemical measurements were performed on a CHI 760C electrochemical workstation. A three-electrode system was used with a modified GCE as working electrode, a Pt foil as counter electrode, and a mercury sulfate electrode (MSE) as reference electrode. All potentials were versus RHE unless otherwise specified. All current densities were normalized by the real surface areas of the precious metals (i.e., electrochemically active surface areas)

RESULTS AND DISCUSSION

Figure 1a shows the scanning electron microscope (SEM) image of NPC obtained by selectively dealloying Al from CuAl alloy foils in 1 M NaOH solution for 5 h. It is observed that the ligament and pore sizes are uniformly distributed across the entire sample. The average size of the smooth copper ligaments is ca. 45 nm. The size of the ligament can also be tuned to some extend by varying reaction parameters such as temperature, time, and post-annealing conditions. This 3D nanoporous material provides a flexible substrate for further functionalization with other catalytic metals such as Pt and Pd. X-sight energy-dispersive X-ray spectrometer (EDS) analysis shows that Al is almost completely removed after 5 h of dealloying.

To uniformly decorate the 3D surface of NPC with precious metals such as Pt, we employ a facile in situ hydrometallurgy approach by placing NPC into 0.8 mM H_2PtCl_6 aqueous solution. Upon the mixing, a spontaneous galvanic-replacement reaction occurs, driven by the difference of the equilibrium potentials between $PtCl_6^{2-}$/Pt (0.735 V vs SHE), and

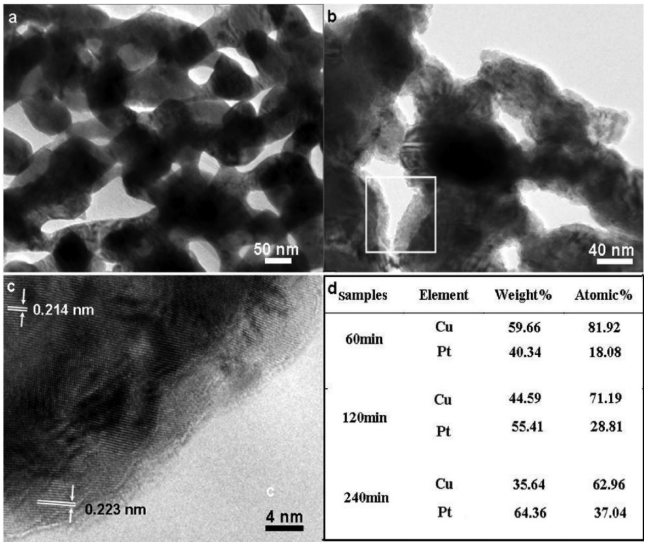

Figure 2. TEM images of (a) NPC and (b) PtCu 60 min sample, (c) HRTEM image of PtCu (60 min), and (d) the compositions of the PtCu sample at different reaction time (results obtained from EDS analysis.

Cu^{2+}/Cu (0.337 V vs SHE). The replacement reaction has been proved to be suitable for deposition of noble metals on different nanoparticles.[11−14] In this process, the yielded $CuCl_2$ salt is highly soluble, which makes the replacement reaction easily proceed. The amount of the loaded Pt can be controlled by reaction time. Figure 1b shows the morphology of the resulted Pt-modified NPC sample fabricated by the replacement reaction for 60 min at 5 °C. It is observed that the resulted composite also shows a 3D nanoporous network structure with slightly coarsened ligaments and rough ligament surface. For further characterization of the NPC-based nanostructure, transmission electron microscope (TEM) image in Figure 2a also reveals the nanoporosity of the NPC sample. After reacting for 60 min, the TEM image in Figure 2b indicates the formation of a thin shell of PtCu alloy on the ligament surface of NPC. The core/shell structure can be identified by the contrast difference between PtCu alloy shell and Cu core. The thickness of the PtCu alloy shell is ca. 3−6 nm. Figure 2c shows the high-resolution TEM (HRTEM) image of the nanocomposite. The clearly-resolved interplanar fringes on the surface are measured to be 0.223 nm, which should be ascribed to the crystal lattice of the (111) planes of face-centered cubic (fcc) Pt-rich PtCu alloy. The reduction of Pt lattice parameters should be due to the substitution of smaller Cu atoms. In the inner part of the ligament, the spacing for adjacent lattice fringes is measured to be 0.214 nm, which corresponds to the value of the (111) planes of fcc Cu. These results demonstrate that the nanocomposite has a Pt-rich PtCu alloy shell and pure Cu core. The HRTEM image also shows a coherent orientation relation between the PtCu alloy shell and the Cu core, indicating that the Pt-rich alloy thin layer grows epitaxially on the Cu ligament. EDS analysis (Figure 2d) demonstrates that the content of Pt in the nanoporous material increases with the increase in reaction time. For the 60-min core/shell structure, the content of Pt is ~18 at %.

X-ray diffraction (XRD) was further used to monitor the evolution of crystal structure of the nanoporous metal during the replacement reaction. As shown in Figure 3, before the reaction the NPC has three diffraction peaks, which are in good

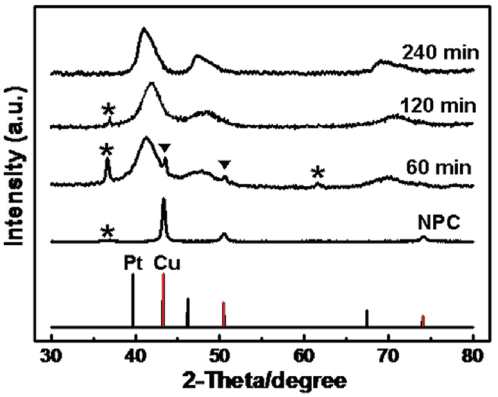

Figure 3. XRD patterns of NPC and the prepared nanocomposites at different reaction time. The standard patterns of pure Pt (JCPDS 65-2868) and Cu (JCPDS 04-0836) are attached for comparison. Weak diffraction peaks from Cu_2O are marked as *.

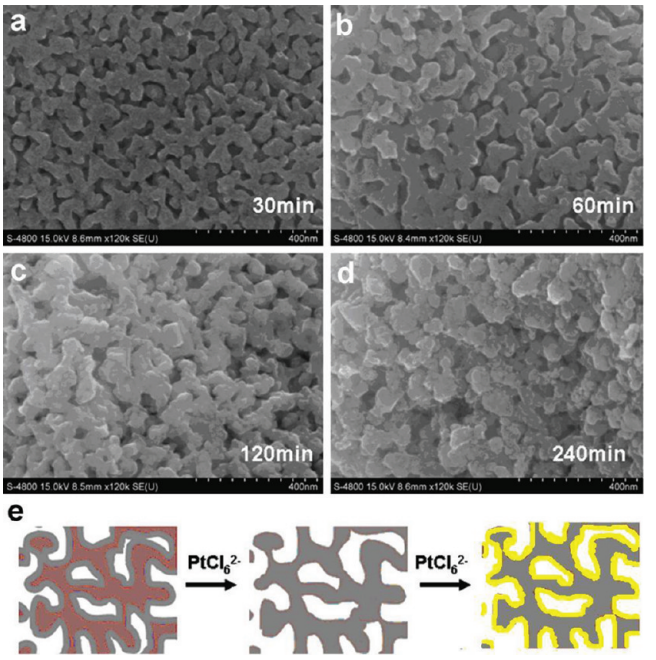

Figure 4. (a−d) SEM images of the nanoporous PtCu nanocomposites at different reaction time. (e) Schematic illustration of structure evolution of the nanocomposites with reaction time.

agreement with those of standard diffractions from pure Cu as denoted by the dotted line. After reacting for 60 min with H_2PtCl_6, the diffraction peaks for Cu (denoted by ▼) are significantly suppressed, and a set of three broad peaks centered at 41.5, 48.5, and 70 (2θ) appear. These three peaks can be ascribed to fcc PtCu alloy, which indicates that although the reaction proceeds at a low temperature (5 °C), the deposited Pt atoms will quickly interdiffuse with the Cu atoms to form a Pt/Cu alloy shell. This observation is actually not unusual because low temperature alloying has been frequently observed for bimetallic nanoparticles.[29] The co-existence of both Pt/Cu alloy and pure Cu further indicates the formation of the core/shell nanostructure. When the reaction time reaches 120 min, the diffraction peaks for pure Cu disappeared, and the three symmetric diffraction peaks can be indexed to disordered single-phase fcc Pt/Cu alloy. The peak position from the (111) diffraction of this sample is in good agreement with the value calculated by Vegard's law (42.26°, this value is calculated based on the data from EDS in Figure 2d). The formation of uniform PtCu alloy ligaments can be explained as follows. After the formation of the core/shell structure (ca. 60 min), the Cu atoms on the surface can still react with Pt salts. As more Cu atoms are leached out, the produced Pt atoms will diffuse into the inner Cu lattices forming uniform PtCu alloy ligaments. When the reaction time reaches 240 min, the three diffraction peaks can also be assigned to an fcc PtCu alloy phase. Compared with the diffraction peaks at 120 min, the diffraction peaks at 240 min shift to lower angles, which indicates that more Pt atoms has been incorporated into the PtCu alloy ligaments. It should be noted that the diffraction peaks related to PtCu alloy are asymmetric with the tail at the higher-angle side, which suggest the formation of a Pt-rich overlayer on the alloy ligament surface.[24] The resulted structure at 240 min should be described as a nanocomposite with a Pt-rich alloy shell and a PtCu alloy core with relatively less Pt content compared with the shell, which can also explain the observed broad XRD diffraction peaks. It is worth mentioning that for the 240 min sample, although we still call it core/shell structure, the clear boundary for core and shell might not exist. This is also the reason that we have not observed separate diffraction peaks from core and shell from the XRD pattern (240 min). As the time further goes, it is observed that the diffraction peaks change negligibly. We assume that this inert Pt-rich alloy shell leads to the termination of the replacement reaction. The appearance of weak diffraction peaks from Cu_2O (denoted by *) should be due to the reaction of nanoscale Cu with O_2 during the sample drying process. The disappearance of Cu_2O at 240 min should be due to the formation of stable Pt-rich alloy.

To understand structure evolution of the core/shell structured nanoporous composite, we also recorded the SEM images of the resulted nanocomposites at different reaction time. As illustrated in Figure 4, after reacting for 30 min, the resulted nanoporous structure is very similar to that of NPC, but due to the deposition of Pt atoms, the ligaments became a little unsmooth (Figure 4a). After reacting for 60 min, the 3D ligament-pore network structure is also well-maintained as stated above; however, the ligaments are obviously coarsened (Figure 4b). After reacting for 120 min, the initial nanoporous structure is slightly broken and some pores are clogged (reduced) by the coarsened ligaments (Figure 4c). With extending the reaction time to 240 min, the nanoporous architecture is significantly damaged, and the sample surface is accumulated with irregular nanoparticles (Figure 4d). The structure evolution of the nanoporous nanocomposites can be explained as follows. At the early stage of the replacement reaction (30 and 60 min), the reaction occurs only at the surface of the Cu ligament forming a Pt/Cu alloy shell and Cu core structure (demonstrated by TEM and XRD). Therefore, the 3D bicontinuous nanoporous structure can be well-maintained. As the reaction time further goes, the continuously produced Pt atoms would diffuse into the inner Cu lattices (at the same time, the inner Cu atoms are leached out), which would make the ligament skeleton unstable and finally damaged. For example, the nanoporous structure is significantly broken after reacting for 240 min.

The whole reaction process and structure evolution can thus be summarized by a schematic illustration (Figure 4e). The structure evolution of the nanoporous metal undergoes three

major steps: core/shell structure with a CuPt alloy shell and Cu core (at 60 min), uniformed PtCu alloy ligament (at 120 min), and core/shell structure with a Pt-rich PtCu alloy shell and Cu-rich PtCu alloy core (at 240 min). At the beginning, as Cu atoms are progressively leached away, the reduced and deposited Pt atoms on the NPC substrate will interdiffuse with surface Cu atoms to form an alloy shell. As the reaction goes on, more Cu atoms will be depleted and the Pt atoms will diffuse into the inner of the Cu ligament to form uniform PtCu alloy. Finally, the surface is passivated due to the formation of a core/shell structure with a Pt-rich PtCu alloy shell and PtCu alloy core with relatively less Pt compared with the shell.

The effects of the experimental parameters such as the concentration of Pt salt and temperature on the resulted structure have also been studied. When Pt salt with a lower concentration (0.4 mM) was used, we observed that instead of the formation of core/shell structure, nanotubular mesoporous Pt/Cu bimetallic material was obtained.[23] By increasing the Pt salt concentration to 0.8 mM, it is interesting to find that novel core−shell nanostructures can be obtained. When further increasing the Pt salt concentration to 1.5 mM, the replacement reaction became very fast and the nanoporous structure was crushed in a short time. The difference in the rate of the replacement reaction should be responsible for the formed different microstructures. Based on both literature results and our study, it is suggested that for the formation of hollow nanostructures such as nanoboxes and nanotubes, a slow galvanic replacement rate is necessary. For example, to prepare AgPd alloy nanboxes, Pd salts were added into Ag nanobox solution by titrating.[30] To prepare CuPd alloy nantubular mesoporous structure in our previous work,[23] low reaction temperature (5 °C) and low Pt salt concentration (0.4 mM) were used. The slow reaction would first start at the most active sites of the nanostructured substrate forming the etch pits. Then, the metal in the inside of the substrate will be oxidized and the reduced nobler metal will be plated on the out surface of the substrate forming hollow alloy nanostructures. In the present work, however, the higher Pt salt concentration used (compared with that in ref 23) would result in a faster replacement reaction. The reaction should occur on the whole nanoporous Cu surface not just the active sites, which results in the formation of core-shell structure. Note that although no etch pits were formed on the nanoporous metal surface, Pt could still diffuse into the inner core forming PdCu alloy with extending the reaction time to 120 min. For the effect of reaction temperature, it was observed that when a higher reaction temperature (60 °C) was used, the bicontinuous nanoporous structure was also crushed after reacting for 60 min. This probably results from the fast deposition of Pt and the greatly enhanced diffusion rate of Cu and Pt.[31] Therefore, to form a uniform core/shell nanoporous structure with controllable metal ratio, a lower temperature is preferred.

The surface states of the as-prepared nanoporous nanocomposites are further studied by electrochemical cyclic voltammetry (CV). Figure 5a shows the CV profiles of the nancomposites (obtained at 60 min, 120 min, and 240 min, respectively) in 0.5 M H_2SO_4 solution. It is observed that with the increase of the replacement reaction time, the hydrogen adsorption/desorption peaks (0.05-0.3 V) become well-defined, the reduction peaks (~0.76 V) for platinum oxides gradually increase in intensity, and the broad Cu dissolution peaks[32] (0.3−0.9 V) markedly decrease. For the 240 min sample, no Cu dissolution can be observed, indicating the formation of a nearly pure Pt surface

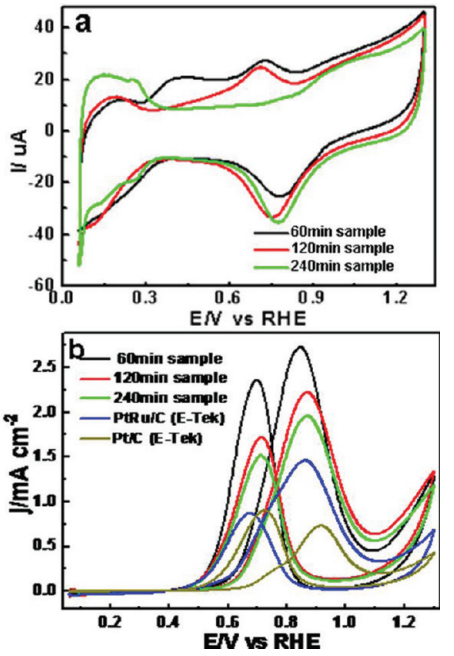

Figure 5. (a) Cyclic voltammograms (CVs) of Pt-based 60, 120, and 240 min samples in 0.5 M H_2SO_4 solution; (b) CVs of the three Pt-based samples, PtRu/C (atomic ration = 1:1) and Pt/C in 0.5 M H_2SO_4 +1.0 M CH_3OH mixed solution. Scan rate: 20 mV/s.

(Pt shell) for this sample. Because EDS analysis (Figure 2d) shows that at 240 min the content of Pt is ~37 at %, the large amount of Cu is clearly in the sublayer core. This result further demonstrates our previous argument that the 240-min sample has a Pt-rich core and Pt/Cu alloy core. Before the electrocatalytic oxidation reaction on the nanocomposites, a pretreatment process (ca. 10 CV scans, see the Experimental Section) was carried out, during which Cu atoms on the alloy shells are slowly dissolved and the left Pt atoms will undergo a reconstruction process to form a nearly pure Pt-shell for all the three samples. Thus, the final core−shell structures have a nearly pure Pt-shell and nearly pure Cu−core (60 min sample) or Pt/Cu alloy−core (120 and 240 min samples). It should be noted that the core−shell structure has not been affected by the electrochemical pretreatment because after the pretreatment, TEM image of the 60 min sample shows no observable changes and EDS analysis only shows a slight decrease in Cu content (for the 60 min sample, the Cu content dropped to ~75 at % from ~81 at %). This result is different from that of electrochemical CV cycling on a Ni−Pt core−shell structure, which can completely dissolve the Ni core forming a hollow Pt nanostructure.[33] The difference should be due to their different reactivity of the core under electrochemical conditions (Cu is more inert).

These nanoporous nanocomposites with low precious metal loading and high surface area should be very desirable for electrocatalysis. We therefore examined their electrocatalytic activities towards methanol electro-oxidation with the aim of evaluating their potential for important energy-conversion technologies, such as direct methanol fuel cells. For comparison, a commercial E-Tek Pt/C catalyst (20 wt % on carbon black) and PtRu catalyst (28 wt % on carbon black) has also been used. Figure 5b shows the CV profiles of the as-prepared nanocomposites and commercial catalysts modified GCE in 0.5 M H_2SO_4 +1.0 M CH_3OH solution. It is observed that the forward anodic peak potentials

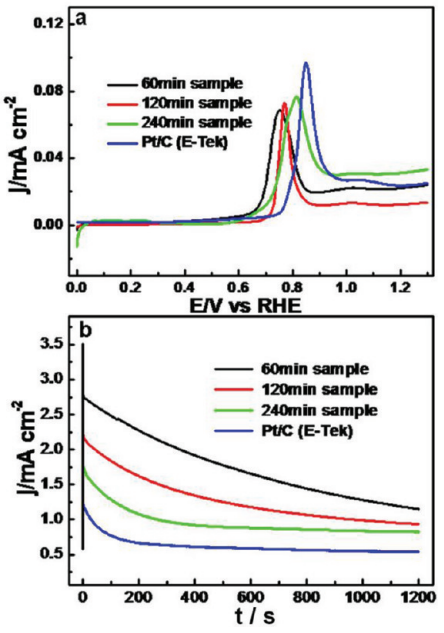

Figure 6. (a) CO-stripping curves recorded in 0.5 M H_2SO_4 solution with a scan rate of 50 mV/s; (b) current−time curves of the Pt-based samples and Pt/C in 0.5 M H_2SO_4 +1.0 M CH_3OH solution at 0.8 V.

are at ∼0.84, ∼0.86, and ∼0.86 V for 60, 120, and 240 min samples, respectively. The peak potentials are at ∼0.86 V for commercial PtRu/C and ∼0.91 V for Pt/C catalyst. The negatively shifted peak potential on the 60 min sample indicates more favorable oxidations of methanol on this sample. Moreover, the specific activity (normalized by the real surface area of Pt) of the 60 min sample is significantly higher than those of other samples. These results indicate the highest catalytic activity of the 60 min sample. The order of the catalytic activity is 60 min sample >120 min sample >240 min sample > PtRu/C > Pt/C. In particular, the specific activity of the 60 min sample is more than three-fold higher than that of Pt/C catalyst. The 60 min sample also shows similar surface specific activity as nanotubular mesoporous PtCu catalyst as reported in our previous work.[23] Since the present Cu/Pt core/shell sample needs shorter reaction time and has lower Pt content, the 60 min core/shell sample holds some advantage compared with the nanotubular mesoporous PtCu catalyst.

To further explore the enhanced electrocatalytic performance of the PtCu nanocomposites, we carried out CO electrostripping experiments. As shown in Figure 6a, the oxidation peak potentials of CO-stripping are at ∼0.74 V for the 60 min sample, ∼0.77 V for the 120 min sample, ∼0.81 for the 240 min sample, and ∼0.85 V for the commercial Pt/C catalyst. The peak currents also increase in the order of 60 min sample < 120 min sample < 240 min sample < Pt/C. The negatively shifted peak potentials and decreased peak currents on the nanocomposites indicate that the adsorbed CO molecules on the nanocomposite surface are weaker than that on Pt/C, i.e., the as-prepared nanocomposites are more tolerant for CO poisoning with the order of the tolerance: 60 min sample > 120 min sample > 240 min sample. This result indicates that the incorporation of Cu with Pt plays an important role for improving the CO tolerance of the Pt shell and the tolerance is depended on Cu content in the core. The highest tolerance of the 60 min sample for CO poisoning also explains why the 60 min sample has the highest activity for methanol oxidation.

The catalytic stability of electrocatalyst is also very important for potential practical applications. Figure 6b shows the current-time curves of the nanocomposites and Pt/C catalyst in 0.5 M H_2SO_4 + 1 M CH_3OH solution at 0.8 V. It is observed that at the beginning the potentiostatic currents decreased quickly for all the catalysts due to the formation of double layer capacitance. Then, the decrease in current should be caused by adsorbed CO-like poisoning species generated by methanol decomposition.[34−36] In addition, adsorption of SO_4^{2-} on the catalyst surface can also inhibit the electrocatalytic reaction.[37,38] It is noted that the current decreases more quickly for Pt/C catalyst, whereas it is slower for the nanocomposits (especially for the 60 min sample). This result indicates that the Pt/C catalyst is quickly poisoned; however, the catalytic activities of the nanocomposites are more stable. The 60 min sample is the most stable one with the highest current density, which is in good agreement with the CV study in Figure 5b.

As to the origin of the enhanced catalytic performance of the PtCu nanocomposites toward methanol electro-oxidation, several points should be mentioned. First, the bicontinuous interconnected porous structure of the nanocomposites provides excellent electron conductivity and also facilitates the mass transfer. Second, the unique core/shell bimetallic structure may allow greatly enhanced catalytic reactivity as a result of possible electronic, strain, or alloy effects.[39] Recently, based on both experimental studies and theoretical calculations, Mavrikakis et al.[40] proved that PtCu near-surface alloy should be a promising catalyst for low-temperature water-gas-shift (WGS) reaction. Zhou et al.[41] reported that Cu/Pt core/shell nanoparticles exhibited very high catalytic activity for NO reduction. Strasser et al.[32,42−48] reported that dealloyed PtCu alloy nanoparticles are excellent electrocatalyst for oxygen reduction. The excellent catalytic activity was suggested to be related to a compressively strained Pt-rich shell. By establishing the activity-strain relationship,[44] they demonstrated experimentally that the deviation of the Pt-shell lattice parameter from that of bulk Pt (i.e., lattice strain in the shell) is the controlling factor in the catalytic enhancement of the dealloyed PtCu alloy nanoparticle which has a similar core/shell structure with the material in this work. On the basis of these arguments, it is no surprise that the present nanoporous core/shell structured nanocomposites exhibit enhanced catalytic activities toward methanol electro-oxidation. The specific activities of the three nanocomposites increase in the order of 240 min sample < 120 min sample < 60 min sample. For all the three samples, a nearly pure Pt shell is formed. Because of the diffusion of Pt atoms into the inner Cu lattices, it has been demonstrated that more Pt will be incorporated into the core as the replacement reaction time increases. Therefore, the difference of the bimetallic ratio in the sub-layer core should be responsible for their different catalytic performance. Strasser et al.[47] have reported that the lattice mismatch between the Pt shell and PtCu core causes a reduced Pt−Pt interatomic distance in the shell. The richer in Cu the core, the smaller its lattice parameter, and hence the more strain induced in the shell.[47] More strain will cause more downward shift of the d-band of Pt.[44] These results explain the higher CO tolerance and catalytic activity of the 60 min sample. In addition, the morphology change of the nanoporous nanocomposites with the reaction time may also contribute to the different catalytic activities. On the other hand, the reduced Pt−Pt interatomic distance (i.e., Pt lattice contraction) should also contribute to the enhanced catalytic stability. In a quite recent study, Wang and

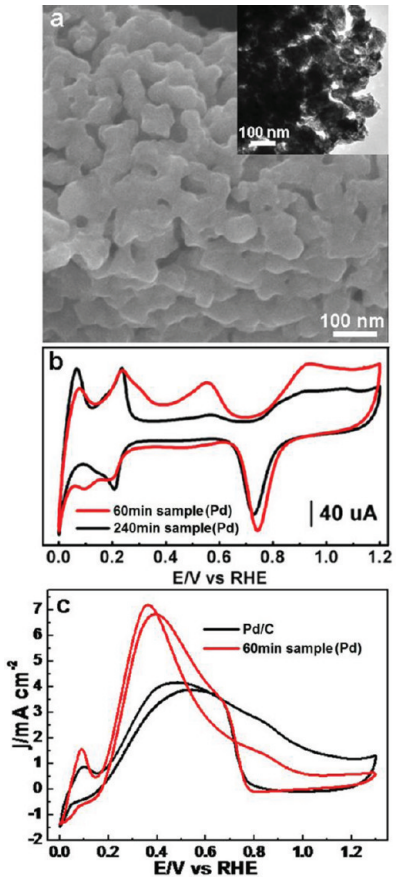

Figure 7. (a) SEM image of the PdCu 60 min sample, inset of (a) is the TEM image of the sample; (b) CVs of Pd-based 60 and 240 min samples in 0.5 M H_2SO_4 solution; (c) CVs of the Pd-based 60 min sample and Pd/C in 0.5 M H_2SO_4 + 0.5 M HCOOH solution. Scan rate: 50 mV/s.

coworkers reported that hollow-induced lattice contraction can remarkably improve the catalytic stability of Pt.[33]

By the same fabrication strategy, Pd-based nanoporous core/shell structure has also been successfully prepared. The morphology and crystal structure evolution of the Pd-based nanoporous nanocomposite with the replacement reaction time are similar to that of Pt-based nanocomposite. Figure 7a shows the SEM image of the 60 min Pd-based sample. It is observed that the pore-ligament structure is retained with relatively coarsened ligament, which is further confirmed by the TEM image (inset of Figure 7a). In the following part of this work, we will focus on the electrochemical properties of the Pd-based nanocomposite. Figure 7b shows the CV profiles of the Pd-based nanocomposites (60 and 240 min samples) in 0.5 M H_2SO_4 solution. For the 60 min sample, it is observed that the hydrogen region is from 0 to 0.3 V with voltammetric profile of hydrogen absorption/desorption and hydrogen evolution. The anodic peak at 0.4-0.7 V can be attributed to the leaching of exposed Cu atoms from the shell surface.[27,49] The cathode peak at ~0.75 V can be ascribed to the reduction of palladium oxide. For the 240 min sample, the hydrogen region becomes well-defined and the Cu dissolution peak disappears, which suggest the formation of a nearly pure Pd-shell on the catalyst surface. These results (similar to the case of Pt) also demonstrate the successfully fabrication of the core/shell structured PdCu nanocomposites.

Figure 7c shows the CV profiles of the PdCu nanocomposite (60 min sample) and commercial Pd/C catalyst in 0.5 M H_2SO_4 + 0.5 M HCOOH solution. It is observed that the current density (normalized by the real surface area of Pd) for HCOOH oxidation on the nanocomposite is much larger than that on the Pd/C. The formic acid oxidation peak on the PdCu nanocomposite also significantly shifts to negative potential compared with that on the Pd/C. These results indicate that the prepared core/shell structured nanocomposite has greatly enhanced electrocatalytic activity toward HCOOH oxidation compared with Pd/C catalyst.

CONCLUSION

By the combination of the dealloying strategy and replacement reaction, we have successfully fabricated nanoporous core/shell structure with Pt(Pd)/Cu alloy shell and Cu (or Pt(Pd)/Cu alloy) core. The thickness of the alloy shell and the metal component of the core can be controlled by changing the replacement reaction time. This inexpensive nanoporous core/shell structured nanocomposites exhibit greatly enhanced electrocatalytic activity and stability for oxidation of small organic molecules, which suggests their potential applications in fell cells and electrochemical sensors. Moreover, this simple and green fabrication strategy is suitable for large-scale production of this novel nanoporous core/shell structured materials.

AUTHOR INFORMATION

Corresponding Author

*Corresponding Author: Prof. H. Qiu, E-mail: qiuhuajun@gmail.com.

ACKNOWLEDGMENT

This work was supported by the National Science Foundation of China (51001053, 50871047), and the Natural Science Foundation of Shandong Province (ZR2010EQ039, ZR2010ZM071). H.Q. thanks the three reviewers for their insightful advice.

REFERENCES

(1) Guo, Y. G.; Hu, J. S.; Zhang, H. M.; Liang, H. P.; Wan, L. J.; Bai, C. L. *Adv. Mater.* **2005**, *17*, 746–750.
(2) Gao, H.; Xiao, F.; Ching, C. B.; Duan, H. *ACS Appl. Mater. Interfaces* **2011**, *3*, 3049–3057.
(3) Park, J.; Cheon, J. *J. Am. Chem. Soc.* **2001**, *123*, 5743–5746.
(4) Chen, M. S.; Kumar, D.; Yi, C. W.; Goodman, D. W. *Science* **2005**, *310*, 291–293.
(5) Zhong, C. J.; Maye, M. M. *Adv. Mater.* **2001**, *13*, 1507–1511.
(6) Habas, S. E.; Lee, H.; Radmilovic, V.; Somorjai, G. A.; Yang, A. P. *Nature Mater.* **2007**, *6*, 692–697.
(7) Zhou, S. H.; Jackson, G. S.; Eichhorn, B. *Adv. Funct. Mater.* **2007**, *17*, 3099–3104.
(8) Sanedrin, R. G.; Georganopoulou, D. G.; Park, S.; Mirkin, C. A. *Adv. Mater.* **2005**, *17*, 1027–1031.
(9) Liu, L. F.; Pippel, E.; Scholz, R.; Gosele, U. *Nano Lett.* **2009**, *9*, 4352–4358.
(10) Gong, K.; Su, D.; Adzic, R. R. *J. Am. Chem. Soc.* **2010**, *132*, 14364–14366.
(11) Wang, J. X.; Inada, H.; Wu, L.; Zhu, Y.; Choi, Y.; Liu, P.; Zhou, W. P.; Adzic, R. R. *J. Am. Chem. Soc.* **2009**, *131*, 17298–17302.
(12) Sasaki, K.; Naohara, H.; Cai, Y.; Choi, Y.; Liu, P.; Vukmirovic, M. B.; Wang, J. X.; Adzic, R. R. *Angew. Chem., Int. Ed.* **2010**, *49*, 8602–8607.
(13) Zhang, J.; Vukmirovic, M. B.; Xu, Y.; Mavrikakis, M.; Adzic, R. R. *Angew. Chem. Int. Ed.* **2005**, *44*, 2132–2135.
(14) Shao, M.; Sasaki, K.; Marinkovic, N. S.; Zhang, L.; Adzic, R. R. *Electrochem. Commun.* **2007**, *9*, 2848–2853.

(15) Barmatov, E. B.; Pebalk, D. A.; Barmatova, M. V. *Langmuir* **2004**, *20*, 10868–10871.
(16) Burda, C.; Chen, X.; Narayanan, R.; El-Sayed, M. *Chem. Rev.* **2005**, *105*, 1025–1102.
(17) Erlebacher, J.; Aziz, M.; Karma, A. *Nature* **2001**, *410*, 450–453.
(18) Qiu, H. J.; Xu, C. X.; Huang, X. R.; Ding, Y.; Qu, Y. B.; Gao, P. J. *J. Phys. Chem. C* **2009**, *113*, 2521–2525.
(19) Yin, H. M.; Zhou, C. Q.; Xu, C. X.; Liu, P. P.; Xu, X. H.; Ding, Y. *J. Phys. Chem. C* **2008**, *112*, 9673–9678.
(20) Xu, C. X.; Su, J. X.; Xu, X. H.; Liu, P. P.; Zhao, H. J.; Tian, F.; Ding, Y. *J. Am. Chem. Soc.* **2007**, *129*, 42–43.
(21) Zhang, J. T.; Liu, P. P.; Ma, H. Y.; Ding, Y. *J. Phys. Chem. C* **2007**, *111*, 10382–10388.
(22) Yoo, S. H.; Park, S. *Adv. Mater.* **2007**, *19*, 1612–1615.
(23) Xu, C. X.; Wang, L.; Wang, R.; Wang, K.; Zhang, Y.; Tian, F.; Ding, Y. *Adv. Mater.* **2009**, *21*, 2165–2169.
(24) Xu, C. X.; Zhang, Y.; Wang, L.; Xu, L.; Ma, H.; Ding, Y. *Chem. Mater.* **2009**, *21*, 3110–3116.
(25) Chen, L. Y.; Fujita, T.; Ding, Y.; Chen, M. W. *Adv. Funct. Mater.* **2010**, *20*, 2279–2285.
(26) Qiu, H. J.; Lu, L.; Huang, X. R.; Zhang, Z.; Qu, Y. *Bioresour. Technol.* **2010**, *101*, 9415–9420.
(27) Liu, A.; Geng, H.; Xu, C.; Qiu, H. *Anal. Chim. Acta* **2011**, *703*, 172–178.
(28) Xu, X.; Liu, Y.; Su, F.; Liu, A.; Qiu, H. *Biosens. Bioelectron.* **2011**, *27*, 160–166.
(29) Shibata, T.; Bunker, B. A.; Zhang, Z. Y.; Meisel, D.; Vardeman, C. F.; Gezelter, J. D. *J. Am. Chem. Soc.* **2002**, *124*, 11989–11996.
(30) Chen, J.; Wiley, B.; McLellan, J.; Xiong, Y.; Li, Z. Y.; Xia, Y. N. *Nano Lett.* **2005**, *5*, 2058–2062.
(31) Song, Y. J.; Doomes, E. E.; Prindle, J.; Tittsworth, R.; Hormes, J.; Kumar, C. S. S. R. *J. Phys. Chem. B* **2005**, *109*, 9330–9338.
(32) Koh, S.; Strasser, P. *J. Am. Chem. Soc.* **2007**, *129*, 12624–12625.
(33) Wang, J. X.; Ma, C.; Choi, Y. M.; Su, D.; Zhu, Y.; Liu, P.; Si, R.; Vukmirovic, M. B.; Zhang, Y.; Adzic, R. R. *J. Am. Chem. Soc.* **2011**, *133*, 13551–13557.
(34) Bai, L.; Zhu, H.; Thrasher, J. S.; Street, S. C. *ACS Appl. Mater. Interface* **2009**, *1*, 2304–2311.
(35) Prabhuram, J.; Zhao, T. S.; Tang, Z. K.; Chen, R.; Liang, Z. X. *J. Phys. Chem. B* **2006**, *110*, 5245–5252.
(36) Kabbabi, A.; Faure, R.; Durand, R.; Beden, B.; Hahn, F.; Leger, J. M.; Lamy, C. *J. Electroanal. Chem.* **1998**, *444*, 41–53.
(37) Guo, J. W.; Zhao, T. S.; Prabhuram, J.; Chen, R.; Wong, C. W. *Electrochim. Acta* **2005**, *51*, 754–763.
(38) Jiang, J.; Kucernak, A. *J. Electroanal. Chem.* **2003**, *543*, 187–199.
(39) Stamenkovic, V. R.; Mun, B. S.; Mayrhofer, K. J. J.; Ross, P. N.; Markovic, N. M. *J. Am. Chem. Soc.* **2006**, *128*, 8813–8819.
(40) Knudsen, J.; Nilekar, A. U.; Vang, R. T.; Schnadt, J. E.; Kunkes, L.; Dumesic, J. A.; Mavrikakis, M.; Besenbacher, F. *J. Am. Chem. Soc.* **2007**, *129*, 6485–6490.
(41) Zhou, S. H.; Varughese, B.; Eichhorn, B.; Jackson, G.; Ilwrath, K. M. *Angew. Chem. Int. Ed.* **2005**, *44*, 4539–4543.
(42) Mani, P.; Srivastava, R.; Strasser, P. *J. Phys. Chem. C* **2008**, *112*, 2770–2778.
(43) Mani, P.; Srivastava, R.; Strasser, P. *J. Power Source* **2011**, *196*, 666–673.
(44) Srivastava, R.; Mani, P.; Strasser, P. *J. Power Source* **2009**, *190*, 40–47.
(45) Srivastava, R.; Mani, P.; Hahn, N.; Strasser, P. *Angew. Chem. Int. Ed.* **2007**, *46*, 8988–8991.
(46) Yang, R.; Leisch, J.; Strasser, P.; Toney, M. F. *Chem. Mater.* **2010**, *22*, 4712–4720.
(47) Strasser, P.; Koh, S.; Anniyev, T.; Greeley, J.; More, K.; Yu, C.; Liu, Z.; Nordlund, S. D.; Ogasawara, H.; Toney, M. F.; Nilsson, A. *Nat. Chem.* **2010**, *2*, 454–459.
(48) Liu, Z.; Koh, S.; Yu, C.; Strasser, P. *J. Electrochem. Soc.* **2007**, *154*, B1192–B1199.
(49) Xu, C.; Liu, A.; Qiu, H.; Liu, Y. *Electrochem. Commun.* **2011**, *13*, 766–769.